JOURNAL OF GEOPHYSICAL RESEARCH, VOL. 100, NO. C2, PAGES 2659–2672, FEBRUARY 15, 1995

Biogeochemical cycling in the global ocean 1. A new, analytical model with continuous vertical resolution and high-latitude dynamics

Gary Shaffer

Department of Geophysics, University of Copenhagen, Copenhagen, Denmark

Jorge L. Sarmiento

Program in Atmosphere and Oceanic Sciences, Princeton University, Princeton, New Jersey

Abstract. A new, simple analytical model of ocean chemistry is presented which includes continuous vertical resolution, high-latitude dynamics, air-sea exchange and sea ice cover. In this high-latitude exchange/interior diffusion-advection (HILDA) model, ocean physics are represented by four parameters: k and w, an eddy diffusion coefficient and a deep upwelling velocity in the stratified interior; q, a rate of lateral exchange between the interior and a well-mixed, deep polar ocean; and u, an exchange velocity between surface and deep layers in the polar ocean. First, estimates are made of ice-free and ice-covered areas at high latitudes, surface temperatures, and air-sea exchange velocities from available data. Then values of the physical parameters are estimated from simultaneous, least mean square fits of model solutions for temperature (T) and "abiotic" carbon 14 ($\Delta^{14}C$) to interior profiles of T and $\Delta^{14}C$ and surface layer $\Delta^{14}C$ values all derived from available data. Best fit values for k, w, q, and u are 3.2×10^{-5} m^2 s^{-1}, 2.0×10^{-8} m s^{-1}, 7.5×10^{-11} s^{-1} and 1.9×10^{-6} m s^{-1} respectively. These results are interpreted in terms of modes of ocean circulation and mixing and compared with results from other simplier and more complex models. In parts 2 and 3 of this series, these values for k, w, q and u are taken as inputs for studying phosphorus, oxygen, and carbon cycling in the global ocean with the HILDA model.

Introduction

There are a number of trace gases which have a major impact on the Earth's radiation balance and climate, and whose atmospheric concentrations are strongly affected by the nature and intensity of biogeochemical cycling in the ocean. The most studied of these is CO_2 but there are others, such as dimethylsulfide (DMS) and N_2O, which may also be of importance. Ice core measurements have confirmed large natural variations in CO_2 concentrations [e.g., *Neftel et al.*, 1982; *Barnola et al.*, 1987] which probably played a major role in climate change over ice age cycles [e.g., *Manabe and Bryan*, 1985]. Mechanisms for such variations in CO_2 concentrations should be sought in the ocean, by far the largest global reservoir of mobile carbon [*Broecker*, 1982; *Bolin*, 1986].

In recent years, two basic groups of simple models have emerged to deal with biogeochemical cycling in the ocean. One group is designed to meet the need for high vertical resolution [e.g., *Oeschger et al.*, 1975; *Volk and Hoffert*, 1985; *Shaffer*, 1989]; the other, to meet the need to consider high-latitude dynamics [e.g., *Sarmiento and Toggweiler*, 1984; *Siegenthaler and Wenk* 1984; *Knox and McElroy*, 1984]. These models have the virtue of being able to reproduce many large-scale features of ocean geochemistry with a very small number of free parameters. Simple models such as these will continue to be of great importance in understanding the chemical dynamics of the ocean, both because of the long time-scales involved and because of the need for large numbers of sensitivity studies. We have thus concluded that it was worth significant effort to go the next logical step in development of such models by combining vertical resolution with high-latitude dynamics in a single model.

Coarse-resolution box models cannot deal successfully with the time-dependent, CO_2 uptake problem [*Oeschger* et al., 1975]. Good vertical resolution is also imperative for steady state models of the oceanic carbon cycle. In general, models with high vertical resolution are needed because rates of important biogeochemical processes may depend upon concentrations. For the carbon cycle, the rate of exchange of inorganic carbon across the sediment-water interface will depend upon the carbonate ion concentration in the adjacent seawater, not upon some deep-sea box average. For the N, O, and S cycles, the nature of the

Paper number 94JC01167.
0148-0227/95/94JC-01167$05.00

chemical reactions involved in organic decomposition at any level in the ocean will depend upon the O_2 and NO_3 concentration at that level [*Shaffer*, 1989].

It is important to include high-latitude processes in models of ocean biogeochemical cycling because the polar surface layer is a window for the atmosphere to the carbon pool of the deep ocean and a window for the deep ocean to the oxygen pool of the atmosphere. Atmospheric pCO_2 and deep ocean O_2 concentrations increase with increased exchange between surface and deep layers at high latitudes and decrease with increased new production in the polar surface layer. Nutrient concentrations in this layer (preformed nutrients) are a diagnostic of how open the window is [*Sarmiento and Toggweiler*, 1984].

Thus a realistic model of ocean chemistry must include both high vertical resolution and high-latitude dynamics. Simple models of this type have been lacking. An outcrop-diffusion model for CO_2 uptake which allowed the deep ocean to impinge upon the polar sea surface [*Siegenthaler*, 1983] was one step in the right direction. Still, the observed high-latitude surface layer should be treated explicitly for CO_2 uptake to consider the influence of ocean mixing and advection on the rate of exchange between the atmosphere and the deep ocean at high latitudes. In a steady state model, a polar surface layer is needed to deal with the high-latitude processes discussed above.

Here we present a new model of ocean chemistry which meets the above requirements. In addition to a high-latitude surface layer, we consider a well-mixed, deep polar ocean, distinct from the stratified interior but interacting with it through lateral exchange. The formulation and use of this exchange is an important advance. It is the link with which we merge a one-dimensional, advection-diffusion model and a box model with high-latitude dynamics into a unified model of ocean chemistry. By fitting our simple high-latitude exchange/interior diffusion-advection (HILDA) model to available ocean tracer data, we can learn something about the physics and biology of the ocean. In particular, the model can make good use of information contained in the high vertical resolution of data sets like that of the Geochemical Ocean Sections Study (GEOSECS).

The goal with this work is to develop simple but general models of the P, N, O, S, and C cycles. Such models have an important role to play in oceanographic, paleoceanographic, and climatic research. This is the first paper in a three-paper series on biogeochemical cycling in the global ocean with emphasis on the natural carbon cycle. Here the HILDA model is presented and applied to two essentially abiotic tracers, temperature and "big delta" carbon 14. Then the physical parameters of the model are calibrated by least mean square fits to ocean-averaged T and $\Delta^{14}C$ data. In paper 2, two biotic tracers, PO_4-P and O_2, are modeled, and biological parameters for the oceanic organic pump are calibrated from PO_4 and O_2 data given the "physics" from paper one. In paper 3, alkalinity is modeled and parameters characterizing the $CaCO_3$ pump are calibrated from alkalinity data given the "physics" and "biology" from papers 1 and 2. Finally, solutions for total inorganic C and atmospheric pCO_2 are obtained and compared with data.

The HILDA Model

Our hybrid, ocean model is shown in Figure 1. A stratified interior I of depth D and width $1-\delta$ is bounded above by a surface layer LS and on the side by a deep, well-mixed, polar layer HD of depth D and width δ, the portion of total ocean area at high latitudes. The HD layer is topped by a high-latitude surface layer HS. The part of this surface layer free from sea ice is δ_s. All regions are connected by the deep, thermohaline circulation characterized by a constant, upwelling velocity w in the interior. Vertical exchange within the interior is parameterized by a constant coefficient of vertical turbulent diffusion, k. Bidirectional exchange between surface and deep polar boxes is proportional to a constant exchange velocity, u. Bidirectional exchange between the deep polar box and any level in the interior depends on a rate of lateral exchange, q. Finally, two-way exchange between the atmosphere and the low- and high-latitude surface layers of the ocean depends on gas exchange velocities g_{LS} and g_{HS}. Bidirectional exchange between the thin low- and high-latitude surface layers is neglected as is gas exchange through sea ice. In the discussion section we relate w and q to different modes of ocean ventilation.

With these physics and the vertical coordinate z defined positive upward, the steady, conservation equation for a tracer ϕ in the interior, $\phi_I(z)$, is

$$k d^2\phi_I(z)/dz^2 - w d\phi_I(z)/dz - q(\phi_I(z)-\phi_{HD}) + S_I(z) = 0 \quad (1)$$

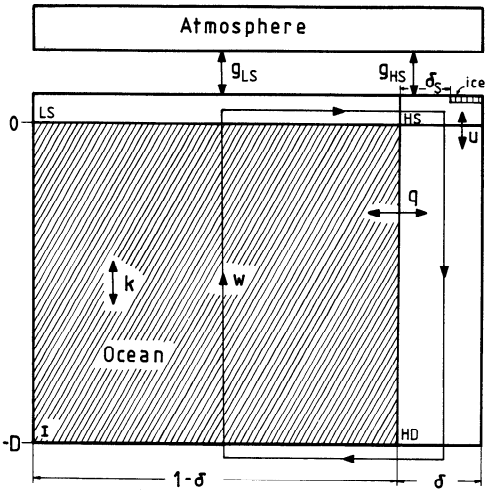

Figure 1. Schematic view of the high latitude exchange/interior diffusion-advection (HILDA) model with a continuously stratified interior I, a deep, well-mixed polar ocean HD and low- and high-latitude surface layers (LS,HS) which interact with the atmosphere.(See text for a more complete description.)

where ϕ_{HD} is the concentration in the deep polar box and $S_I(z)$ is the distribution of sources and sinks in I.

In the deep polar box, conservation of ϕ demands

$$(1-\delta)w(\phi_{HS}-\phi_{HD}) + \delta u(\phi_{HS}-\phi_{HD}) + (1-\delta)q\int_{-D}^{0}(\phi_I(z)-\phi_{HD})dz + \delta S_{HD} = 0 \quad (2)$$

where ϕ_{HS} is the concentration in the high-latitude surface box and S_{HD} describes sources and sinks in the HD box. We may write

$$q\int_{-D}^{0}(\phi_I(z)-\phi_{HD})dz = qD(\langle\phi_I\rangle(z)-\phi_{HD}) \quad (3)$$

where $\langle\phi_I\rangle(z)$ is the interior average; qD can be identified as a exchange velocity, and the analogy to simplier box model formulations is clear.

For the low-latitude surface box,

$$g_{LS}(\phi_A-\phi_{LS}) - kd\phi_I(z)/dz|_{z=o} + [w(\phi_I(z)|_{z=o}-\phi_{LS})] + S_{LS} = 0 \quad (4)$$

where ϕ_A and ϕ_{LS} are concentrations in the atmosphere and in the LS box, respectively. S_{LS} describes sources and sinks in the LS box. Equation (4) may also be considered as an upper boundary condition on the interior. A second relationship between the interior and the LS box is the matching condition,

$$\phi_I(z) - \phi_{LS} = 0, \quad z=0 \quad (5)$$

which follows from our formulation of ocean physics. Given (5), the advective term in square brackets in (4) drops out.

For the high-latitude surface box,

$$\delta_S g_{HS}(\phi_A-\phi_{HS}) + (1-\delta)w(\phi_{LS}-\phi_{HS}) - \delta u(\phi_{HS}-\phi_{HD}) + \delta S_{HS} = 0 \quad (6)$$

where S_{HS} describes sources and sinks in the HS box. In the steady state, the thicknesses of the surface layers enter the problem formulated here only if surface layer sources and sinks depend upon these thicknesses.

The problem is closed by specification of the bottom boundary condition on the interior. The proper condition is that the net flux out of the bottom boundary balances the net influx plus net sources on the bottom or

$$kd\phi_I(z)/dz - w(\phi_I(z)-\phi_{HD}) + S_B = 0, \quad z=-D \quad (7)$$

where S_B describes sources and sinks on the ocean bottom. This is equivalent to considering a bottom box governed by equations like (4) and (5). Sources and sinks on the bottom of the HD box are included in S_{HD} of (2).

Analytical Solutions For Temperature And Carbon 14

Temperature

The general solution of (1) for the interior temperature with $S_I(z)=0$ is

$$T_I(z) = T_{HD} + A_1\exp(s_1 z) + B_1\exp(s_2 z) \quad (8)$$

where $s_1, s_2 = 0.5[wk^{-1} \pm (w^2k^{-2}+4qk^{-1})^{1/2}]$.

In the following, the surface layer temperatures T_{LS}, T_{HS}, are prescribed for simplicity. A proper treatment of surface layer heat balances would require input from an interactive atmospheric model and is beyond the scope of the present paper. Application of conditions (5) and (7) given (8) and $S_B = 0$ (neglect of weak geothermal heating) yields (A1) and (A2) in the appendix. A third algebraic equation relating T_{HD}, A_1, and B_1 can be obtained from conservation of heat in the deep polar box (2) with $S_{HD} = 0$ and the overall heat balance of the interior, yielding the condition of no net heat flux to the deep ocean,

$$w(T_{HS}-T_{LS}) + \delta(1-\delta)^{-1}u(T_{HS}-T_{HD}) + kdT_I(z)/dz|_{z=0} = 0 \quad (9)$$

Equation (A3) obtains from (8) and (9).

The solution of (A1)-(A3) for the temperature in the deep polar box is

$$T_{HD} = a_1T_{LS} + a_2T_{HS} \quad (10)$$

where

$a_1 = a_3^{-1}[(1-s_2s_1^{-1}) + a_4(1-w(ks_1)^{-1})]$,

$a_2 = a_3^{-1}[a_4(ks_1)^{-1}(w + \delta(1-\delta)^{-1}u)]$,

$a_3 = 1 - s_1s_2^{-1} + a_4[1 + \delta(ks_1(1-\delta))^{-1}u]$,

$a_4 = (w-ks_2)\exp(-s_2D)[(w-ks_1)\exp(-s_1D)]^{-1}-1$.

A_1 and B_1 for the interior profile follow accordingly.

In the limit of no horizontal ventilation between the interior and the deep polar box ($q \to 0$), $s_1 \to wk^{-1}$ and $s_2 \to 0$. Then from (A1)-(A3), $T_{HD} \to T_{HS}$, since the deep polar box cannot now be heated via the interior in this limit. Also, $A_1 \to T_{LS} - T_{HS}$ and $B_1 \to 0$. Thus the interior temperature follows the one-dimensional, advective-diffusive, "pipe" model solution [cf. *Shaffer*, 1989]. In the limit $q, w \to 0$, the diffusive interior and the deep polar box become decoupled. Both become isothermal, each with the temperature of the surface layer above it. The interested reader may identify and work out several other subcases for temperature (and for carbon 14 considered below).

Carbon 14

It is appropriate to express the carbon 14 content at any point in the ocean as a $^{14}C/^{12}C$ ratio when, as here, carbon 14 is to be used as a tracer. Although ^{14}C is transported

downward with the rain of organic particles produced by marine organisms, use of $^{14}C/^{12}C$ ratios tends to cancel the effect of this biotic transport because both isotopes are fixed in organic form and metabolized back to inorganic form. Thus we will use the ^{13}C fractionation-corrected ratio of $^{14}C/^{12}C$ [cf. *Siegenthaler*, 1986] here, and ^{14}C will be used henceforth to refer to this ratio. The error introduced in neglecting biological effects with this approach is less than 10% of the signal produced by circulation and radioactive decay [*Fiadeiro*, 1982; *Bacastow and Maier-Reimer*, 1990].

In the model calculation we introduce an arbitrary scale for ^{14}C such that atmospheric ^{14}C is one unit. Before presenting model results we convert to standard $\Delta^{14}C$ units as follows:

$$\Delta^{14}C = 1000(\text{model units} - 1) \tag{11}$$

Since we consider steady state solutions for ^{14}C, we will compare with reconstructions of preindustrial distributions of $\Delta^{14}C$. We take $\Delta^{14}C$ in the preindustrial atmosphere to be 0 ‰.

For the ^{14}C problem formulated above, $S_I(z) = -\lambda^{14}C_I(z)$, where λ, the radioactive decay rate for carbon 14, is 3.84×10^{-12} s^{-1}. Then the general solution of (1) for ^{14}C in the interior is

$$^{14}C_I(z) = q(q+\lambda)^{-1}\,{}^{14}C_{HD} + A_2\exp(s_3 z) + B_2\exp(s_4 z) \tag{12}$$

where s_3, $s_4 = 0.5[wk^{-1} \pm (w^2 k^{-2} + 4(q+\lambda)k^{-1})^{1/2}]$.

Given $S_B = 0$ for the present abiotic approach, conditions (5) and (7) together with (12) yield (A4) and (A5) in the appendix. To an excellent approximation we can neglect radioactive decay in the thin surface layers. Then we have S_{LS}, $S_{HS} = 0$ and from (4) and (6), we get (A6) and (A7).

A convenient form of the fifth equation relating $^{14}C_{LS}$, $^{14}C_{HS}$, $^{14}C_{HD}$, A_2, and B_2 is obtained from the conservation equation for the deep polar box (2), where $S_{HD} = -\lambda D^{14}C_{HD}$, and the net air-sea exchange - radioactive decay balance,

$$(1-\delta)g_{LS}(1-{}^{14}C_{LS}) + \delta_S g_{HS}(1-{}^{14}C_{HS}) - (1-\delta)\lambda\int_{-D}^{0} {}^{14}C_I(z)dz - \delta\lambda D^{14}C_{HD} = 0 \tag{13}$$

After manipulation of (2) and (13) to cancel terms involving the vertical integral of $^{14}C_I(z)$, we get (A8).

Equations (A4)-(A8) can be solved by substitution for the five unknowns in terms of δ, δ_S, g_{LS}, k, w, q and u. For brevity, however, the complicated expressions that result will not be presented here. In the limit of no horizontal ventilation ($q \to 0$), high- and low-latitude ^{14}C concentrations remain coupled, and, as a result of advection, the balance between atmospheric source and oceanic sink is not local. In the limit q, $w \to 0$, high- and low-latitude oceans are again decoupled. The resulting case of a diffusive interior has been treated elsewhere [*Oeschger* et al., 1975] and the solution for the two-box polar region is an easy exercise.

Estimates of Physical Parameter Values for the Modern Ocean

Choice of External Parameters

Specific model solutions for temperature and carbon 14 depend upon the parameters k, w, q, and u, which define the physics of our model ocean, and upon external parameters. The latter are δ and δ_S (width of total and ice-free polar zone), T_{LS} and T_{HS} (low and high latitude surface layer temperatures), and g_{LS} and g_{HS} (low and high latitude air-sea exchange velocities). Polar convergences form natural boundaries between low-latitude and polar regimes in the ocean. With the annual mean sea surface temperature $\langle T \rangle (x,y,0)$ in the range 2°-8°C as a marker of these transitions, available data from 1° squares [*Levitus*, 1982] yield δ between 0.112 and 0.211 for the modern ocean. Here we choose $\langle T \rangle (x,y,0) = 5$°C as our polar boundary whereby $\delta = 0.16$. In the Southern Ocean, the polar boundary defined in this way dips to ~60°S south of New Zealand and rises to ~48°S south of Africa. In the North Atlantic, $\langle T \rangle (x,y,0)$ is less than 5°C in the Arctic Ocean, in the western Norwegian Sea, and off the coasts of Greenland and Labrador. In the North Pacific, only the Bering Sea and waters off Kamchatka are polar by this definition. Ice cover of our polar zone varies from about one sixth in the summer to about one half in the winter with a yearly mean of somewhat more than one third [*Gordon*, 1981; *Walsh and Johnson*, 1979]. We take $\delta_S = 0.10$ here.

Given the boundary defined by $\langle T \rangle (x,y,0) = 5$°C, we calculated mean potential temperature profiles for a low- and a high-latitude ocean from the 1° square data. Figure 2 shows these temperatures (heavy dots) at chosen depths together with their standard deviations (bars). The polar ocean is quite uniform with a potential temperature range over depth of only ~1°C. This supports our model assumption of a well-mixed, deep polar box. The vertically-averaged potential temperature in the polar region (weighted by area as a function of depth, see below) is 0.80°C. The two potential temperature profile curves in figure 2 will be discussed below.

Yearly mean temperatures in the surface layer, chosen here for simplicity to be the upper 50 m, are 21.00°C and 0.53°C for the low and high latitude oceans respectively. However, these are probably not the most appropriate choices for T_{LS} and T_{HS} here. Strong winds, cold surface temperatures, lack of melt water, and salt exclusion during ice formation promote vertical mixing and convection during winter at mid- and high latitudes. Here we try to account for such correlations between increased vertical exchange and cold surface temperatures by identifying T_{LS} and T_{HS} with wintertime mean surface layer temperatures. From the *Levitus* [1982] data and our boundary defined above, these are 19.54°C and -0.34°C, respectively. Below we test the sensitivity of our results to other choices of T_{LS} and T_{HS}.

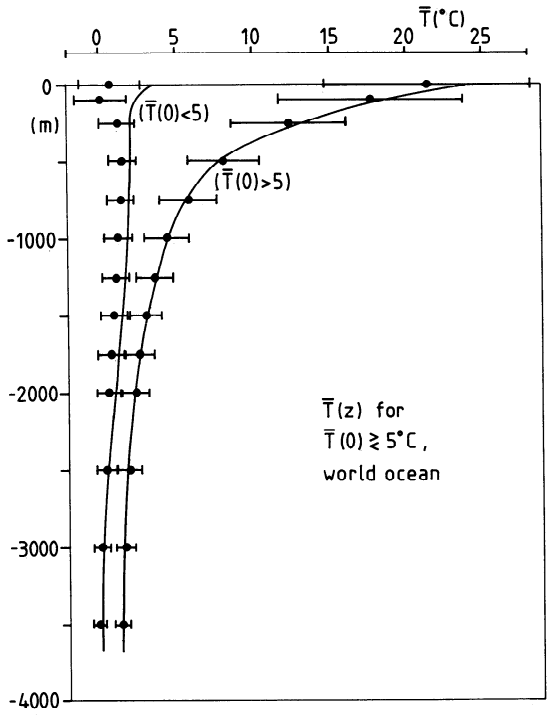

Figure 2. Data-based, mean potential temperatures versus depth for the low-latitude ($T(0)>5$) and high-latitude ($T(0)<5$) ocean. Discrete means (dots) and their standard deviations (bars) are from 1° square data [*Levitus*, 1982]. Continuous profiles are from GEOSECS data.

The overall conservation equation for ^{14}C (13) can be expressed as

$$(1-\delta)g_{LS}(1-{}^{14}C_{LS}) + \delta_S g_{HS}(1-{}^{14}C_{HS}) - \lambda D\langle {}^{14}C\rangle = 0 \quad (14)$$

where $\langle {}^{14}C\rangle$ is a preindustrial, ocean mean value. From available $\Delta^{14}C$ data considered below, we estimate $\langle {}^{14}C\rangle$ = 0.84 (i.e., $\Delta^{14}C$ = - 160 ‰). A better expression for exchange of ^{14}C across the high-latitude sea surface would be $\langle \delta_S(t) g_{HS}(t)[1-{}^{14}C_{HS}(t)]\rangle$ where the angle brackets represent yearly averaging. High winds during winter lead to large g_{HS}, perhaps twice as large as typical g_{LS}, but cold temperatures then lead to small δ_S. The product of the two varies less and, in fact, approximates δg_{LS} in size given the ice coverage data above. Here we substitute δg_{LS} for $\delta_S g_{HS}$ throughout, a simplication which eliminates both δ_S and g_{HS} from the present problem. Then with D = 3800 m, the mean ocean depth, we have

$$g_{LS} = 1.23\text{x}10^{-8}\text{m s}^{-1}[(1-\delta)(1-{}^{14}C_{LS}) + \delta(1-{}^{14}C_{HS})]^{-1} \quad (15)$$

Given any two of g_{LS}, $^{14}C_{LS}$, and $^{14}C_{HS}$, (15) can be solved for the third. Gas exchange velocities derived by other methods, i.e., from radon data [*Peng* et al., 1979], may diverge substantially from those derived from a ^{14}C conservation approach like the present one [*Siegenthaler*, 1986]. Therefore we choose to estimate $^{14}C_{LS}$ and $^{14}C_{HS}$ and solve for g_{LS} from (15). Prebomb values for $\Delta^{14}C$ in the low-latitude surface layer from direct observations and banded coral data range from about -40 ‰ in subtropical gyres to about -70 ‰ at the equator [*Broecker and Peng*, 1982; *Toggweiler et al.*, 1989]. The change in $\Delta^{14}C$ in the LS layer over the industrial era, due to dilution with fossil fuel CO_2 devoid of carbon 14 (Suess effect), ranges from -6 ‰ at the equator to -13 ‰ in the subtropical gyres from the coral data. These results imply average, preindustrial $\Delta^{14}C$ values in the range -30 ‰ to -50 ‰ in the LS layer. We take $^{14}C_{LS}$=0.96 ($\Delta^{14}C_{LS}$ = -40 ‰) as our standard value.

The few existing prebomb observations of $\Delta^{14}C$ in the high- latitude surface layers indicate a range of -100 ‰ to -140 ‰ for the Southern Ocean and values exceeding -100 ‰ for the North Atlantic [*Broecker and Peng*, 1982]. Deep water end points for the upper water column in these oceans are about -75 ‰ and -150 ‰, respectively [*Stuiver et al.*, 1983]. The Suess effect is probably small (a few per mil) at high latitudes due to strong coupling with the deep ocean. Wintertime bias discussed above would motivate a choice for $\Delta^{14}C_{HS}$ on the low side. We feel that an effective $\Delta^{14}C_{HS}$ for the preindustrial ocean lies in the range -100 ‰ to -140 ‰ and thus will choose $^{14}C_{HS}$ = 0.88 (i.e. $\Delta^{14}C_{HS}$ = -120 ‰) as our standard value.

From (15) with $^{14}C_{LS}$, $^{14}C_{HS}$ = 0.96, 0.88, we get g_{LS} = $2.32\text{x}10^{-7}$ m s^{-1}. The invasion flux of CO_2 is the product of g_{LS} and an ocean mean concentration of total inorganic carbon. Given ΣCO_2 = 2.33 mol m^{-3}, the flux is $5.41\text{x}10^{-7}$ mol C m^{-2} s^{-1} or 17.1 mol C m^{-2} yr^{-1}. This agrees with other estimates based on the ^{14}C conservation approach [*Siegenthaler*, 1986].

Mean $\Delta^{14}C$ profiles

Given the above values for T_{LS} and T_{HS}, the model can reproduce the interior profile of potential temperature (figure 2) well. Least mean square, best fits to this profile place constraints on the ratios of the physical parameters but not on their absolute values. As was first noted by *Munk* [1966], the use of carbon 14 distributions as constraints helps pin down absolute values for physical parameters. The constant decay rate of ^{14}C combined with observed $\Delta^{14}C$ puts strong limits on the rate of ocean flushing and thus also on the physical processes doing the flushing. While Munk's analysis was limited to the deep Pacific, we deal with the whole ocean. Thus we have been able to make use of overall constraints on ^{14}C and apply flux boundary conditions. While Munk worked with one-dimensional, advective-diffusive physics, we consider a model that also allows for lateral ventilation and that can make use of both low- and high-latitude information.

We use the GEOSECS $\Delta^{14}C$ data set, cast into the model configuration, for comparison with model results. First, the total data set was partitioned into low- and high-latitude

subsets by use of the $\langle T \rangle (x,y,0) = 5°C$ boundary. The following GEOSECS stations fall into the high latitude ocean: 6-9 and 15-17 for the North Atlantic and 67-90, 279-294, and 429-433 for the Southern Ocean. The remaining, "low-latitude" stations were partitioned by ocean basin and least mean square, Bi-cubic spline curves with one knot in the vertical were calculated for each basin from the resulting data. Figure 3 shows the data and the spline fits for the North Pacific and North Atlantic. Ocean mean $\Delta^{14}C$ profiles were then formed by combining these curves with the help of weights from ratios of ocean basin area to total ocean area. Since each basin has a different topography, the weights are depth dependent. Table 1 lists absolute areas and weights at selected depths as calculated from the 1° square data [*Levitus*, 1982]. Figure 4 shows the mean $\Delta^{14}C$ profile for the low-latitude ocean (heavy line) along with the spline fits to the data from the six ocean basins. North Atlantic Deep Water can be traced into the Indian Ocean along a deepening $\Delta^{14}C$ maximum. Profiles in and above the main ocean thermocline (depths less than ~ 1000 m) are affected by bomb ^{14}C. Also shown is the estimate of $\Delta^{14}C_{LS}$ presented above. Results for the undersampled polar ocean, which (in particular in the North Atlantic Ocean), may be significantly affected by bomb ^{14}C, are not presented.

To check the representivity of mean profiles based on the GEOSECS data set, mean potential temperature profiles were calculated as above from GEOSECS data (curves in Figure 2). Excellent agreement with mean profiles from the *Levitus* [1982] data (dots in Figure 2) is found below about 300 m in the low-latitude ocean. GEOSECS-based mean potential temperatures exceed those based on the 1° square data by 0.2°-0.6°C in the deep polar ocean. Undersampling probably explains this disagreement. Thus GEOSECS data from above 300 m in the interior and from the polar ocean will not be used to constrain the tracer solutions.

Best Fit Values for the Physical Parameters

On the basis of results presented above, we choose the following information to constrain the physical parameters of the model: the mean, low-latitude profile of potential temperature and the average, high-latitude potential temperature from the 1° square data, the mean $\Delta^{14}C$ profile for the low latitude ocean from 1000 m downward and estimates of mean, preindustrial $\Delta^{14}C$ in the low- and high-latitude surface layers. Interior profiles are resolved well enough by discrete values at 250-m intervals. In the model, z=0 corresponds to the base of the surface layer. Here we compare model results at z=250 with data from 300 m and so on given an assumed surface layer thickness of 50 m.

Table 2 lists the resulting data constraints for the standard case. Given the above values for the external parameters, model solutions were obtained for specific choices of k, w, q, and u and model results corresponding to the data constraints were extracted. After transformation of ^{14}C results to the Δ notation, we formed the residual

$$R = \sum_{i=1}^{16} [(\langle T_i \rangle - T_i)(20°C)^{-1}]^2 + \sum_{i-17}^{31} [(\langle \Delta^{14}C_i \rangle - \Delta^{14}C_i)(180\ ‰)^{-1}]^2 \quad (16)$$

where angle brackets indicate data constraints. Here the data from the LS, HS and HD layers were counted twice; i.e., they were given a weight corresponding to 500 m of interior profile data. T and $\Delta^{14}C$ differences in (16) have been divided by scaling factors representing observed ranges of T and $\Delta^{14}C$. A search of k, w, q, and u space for the minimum of R yielded the following standard case, best fit values (subscript B) for the physical parameters:

$$k_B = 3.2 \times 10^{-5}\ m^2\ s^{-1}, \quad w_B = 2.0 \times 10^{-8}\ m\ s^{-1}$$
$$q_B = 7.5 \times 10^{-11}\ s^{-1}, \quad u_B = 1.9 \times 10^{-6}\ m\ s^{-1}$$

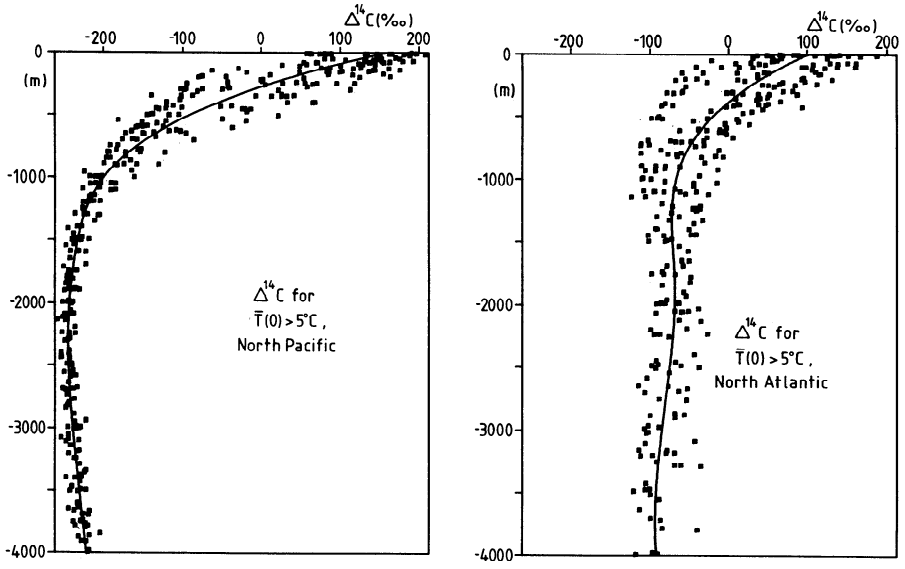

Figure 3. Low-latitude ocean carbon 14 data from the GEOSECS (a) North Pacific and (b) North Atlantic

Table 1. Absolute Areas and Area Fractions by Ocean Basin in the Low Latitude Ocean, as Defined in the Text, for Several Selected Depths.

	North Pacific		South Pacific		North Atlantic		South Atlantic		North Indian		South Indian	
z, m	Area, 10^{13} m^2	Fraction	Area, 10^{13} m^2	Fraction	Area, 10^{13} m^2	Fraction	Area, 10^{13} m^2	Fraction	Area, 10^{13} m^2	Fraction	Area 10^{13} m^2	Fraction
0	7.79	0.259	8.05	0.268	4.43	0.148	3.36	0.112	1.17	0.039	5.21	0.174
1000	7.29	0.263	7.80	0.282	3.69	0.133	3.15	0.114	0.99	0.036	4.75	0.172
2000	7.03	0.268	7.40	0.282	3.35	0.128	3.07	0.117	0.87	0.033	4.49	0.171
3000	6.60	0.280	6.71	0.284	2.83	0.120	2.84	0.120	0.67	0.029	3.97	0.168

Calculations are based on *Levitus* [1982] data

For this best fit solution, model results corresponding to the data constraints are listed in Table 2 and the profiles $T_I(z)$ and $\Delta^{14}C_I(z)$ and are shown in Figures 6 and 7 (middle profiles). Mean deviations of the best fit solution from the data constraints are 0.44°C for temperature and 5.0 ‰ for carbon 14.

The above results are rather insensitive to weighting choices. Doubling or halving the scaling factor of T relative to that of $\Delta^{14}C$ (or vice versa) in (16) only leads to small changes (<10%) in the best fit, physical parameter values. Doubling or halving the weighting of interior profile versus boundary box constraints leads to changes less than 10% in all parameters except w, which increases (decreases) by about 20% when weighting on interior constraints is doubled (halved).

The accuracy of the best fit estimates of any parameter can be studied by fixing that parameter independently and searching for best fit solutions. Figure 5 presents the results of such a calculation as the ratio of the resulting R to the absolute minimum R as a function of each specified parameter. For comparison, the x -axis has been scaled to make the above best fit values for the physical parameters coincide. Within the context of the model, oceanic T and $\Delta^{14}C$ data constrain the vertical diffusion coefficient most strongly, followed by the rate of lateral ventilation. Least constrained are the lower bound on deep upwelling and the upper bound on the high-latitude exchange velocity. Reasons for these differences are discussed below. If we take RR_{min}^{-1} = 1.5 as a worst acceptable fit to the data, the ranges of acceptable parameter values are 2.3-4.1x10^{-5} m^2 s^{-1} for k, 0-3.4x10^{-8} m s^{-1} for w, 4.7-11.8x10^{-11} s^{-1} for q and 1.1-4.0x10^{-6} m s^{-1} for u.

Uncertainty in the values chosen for the external parameters T_{LS}, T_{HS}, $\Delta^{14}C_A$, and δ_S, g_{LS}, and g_{HS} in the data constraints T_{HD}, $\Delta^{14}C_{LS}$, and $\Delta^{14}C_{HS}$ are potential sources of error. Table 3 lists best fit solutions for some different combinations of these parameters and data constraints. If yearly mean temperatures are chosen for the low- and high-latitude surface layers (T_{LS}=21.0, T_{HS}=0.53), best fit solutions result with poorer fit to data, particularly for T_{LS}=21.0. Still, changes in the best fit values of the physical parameters are small (<10%) except for a 50% increase in high-latitude exchange (u). With relatively warm T_{HS}, a larger u is needed to cool the deep ocean. For relatively warm T_{LS}, weaker vertical mixing (k) is required to keep it cold. On the other hand, solutions with colder T_{LS} and T_{HS} (18°C and -1.00°C) fit data better. Such choices might be appropiate in the context of the HILDA model to further account for large vertical exchange concentrated in cold regions of the ocean. Solutions for the deep temperature constraint at high latitudes over a reasonable range of uncertainty,

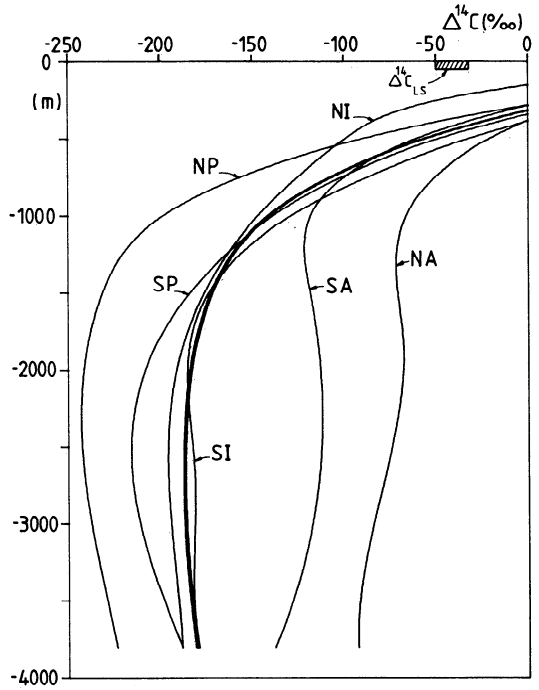

Figure 4. Mean low-latitude ocean profile of carbon 14 (heavy curve) from Bi-cubic spline fits to GEOSECS data from the North and South Atlantic (NA, SA), Pacific (NP, SP) and Indian (NI, SI) oceans (other curves) and the use of area-based weights (Table 1). Also shown is an estimate for mean preindustrial carbon 14 in the low-latitude surface layer ($\Delta^{14}C_{LS}$).

Table 2. Standard Case, Data Constraints for Temperature and Carbon 14 ($\langle T \rangle$, $\langle \Delta^{14}C \rangle$) and Corresponding HILDA Model Results (T, $\Delta^{14}C$) for the Solution With the Least Mean Square, Best Fit to These Constraints According to Equation (16)

z, m	$\langle T \rangle$ (z) °C	$T(z)$, °C	$\langle \Delta^{14}C \rangle$ (z), ‰	$\Delta^{14}C$, ‰
250	11.31	12.87	...	-94.6
500	7.70	8.68	...	-129.3
750	5.63	6.04	...	-150.8
1000	4.39	4.38	-146.1	-164.2
1250	3.60	3.33	-163.8	-172.5
1500	3.07	2.67	-174.1	-177.5
1750	2.67	2.26	-180.5	-180.5
2000	2.42	2.00	-184.5	-182.2
2250	2.16	1.84	-186.5	-182.9
2500	1.98	1.73	-187.3	-183.0
2750	1.82	1.67	-187.4	-182.5
3000	1.67	1.63	-186.7	-181.5
3250	1.54	1.61	-185.4	-179.9
3500	1.42	1.59	-183.3	-177.4

$\langle T \rangle_{HD}$ = 0.80°C, T_{HD} = 1.56°C, $\langle \Delta^{14}C_{LS} \rangle$ = -40 ‰, $\Delta^{14}C_{LS}$ = -39.0 ‰, $\langle \Delta^{14}C_{HS} \rangle$ = -120 ‰, $\Delta^{14}C_{HS}$ = -125.1 ‰, and $\Delta^{14}C_{HD}$ = -145.0 ‰

0.30°C-1.30°C, show little change in best fit values of the physical parameters.

The choice of constraints $\Delta^{14}C_{LS}$ and $\Delta^{14}C_{HS}$ strongly influences the results (note that changes in these values imply changes in air-sea exchange; see equation (15) and Table 3). Both high $\Delta^{14}C_{LS}$ and low $\Delta^{14}C_{HS}$ improve the fit to data. A change in $\Delta^{14}C_{LS}$ affects k_B and w_B, both involved in near-surface dynamics of the low-latitude ocean, but not q_B and u_B. A change in $\Delta^{14}C_{HS}$ affects w_B, q_B, and u_B, all involved in high-latitude dynamics, but not k_B. A new, best fit calculation constrained only by the 25 interior constraints of T and $\Delta^{14}C$ given T_{LS}=19.54°C, T_{HS}= -0.34°C and g_{LS} = 2.32x10^{-7} m s^{-1}, yields 2.8x10^{-5} m^2 s^{-1}, 0 m s^{-1}, 10.7x10^{-11} s^{-1} and 2.5x10^{-6} m s^{-1}, for k_B, w_B, q_B and u_B as well as a low $\Delta^{14}C_{HS}$ of -141.4 ‰. Clearly, constraints on surface layer $\Delta^{14}C$ contribute important information to this inverse problem. Our inability to pin down $\Delta^{14}C_{HS}$ better owing to lack of data is a large source of uncertainty in our results.

Best fit values for our physical parameters are not very sensitive to a reasonable range of ^{14}C levels in the preanthropogenic atmosphere (Table 3). These values change by less than 10% for $\Delta^{14}C_A$ = -5 ‰, near the mean for the last millennium [*Stuiver and Quay*, 1980](note again implied change in g_{LS}). On the other hand, best fit values of k and w are not insensitive to different g_{HS} and/or δ_S. With relatively weak air-sea exchange at high latitudes, for instance, for g_{HS} = g_{LS} with standard δ_S (Table 3, footnote), relatively less ^{14}C enters the ocean at high latitudes. Then net ^{14}C balance (equation (14)) with a fixed ocean mean requires a larger g_{LS} and larger k and w are needed to match increased ^{14}C transport down out of the low-latitude surface layer while retaining interior profile shapes. The converse is true for strong air-sea exchange at high latitudes, for instance, for the case with no or porous [*Fanning and Torres*, 1991] ice cover but standard g_{HS} (Table 3, footnote).

Another way to look at this high-latitude gas exchange effect is to consider changes in surface layer to deep ocean differences in $\Delta^{14}C$ which would arise in the HILDA model solely from changes in g_{HS} or ice cover with the remaining parameters fixed to their best fit or standard values. For the two cases above, which simulate changes in ice cover not unlike glacial to interglacial changes, these differences, referenced to a depth of 2500 m, are -160.9 ‰ and -126.3 ‰ respectively. The value for the standard case difference is -144 ‰ (Table 2). We conclude that it is important to consider this gas exchange effect when $\Delta^{14}C$ data from sediment cores are used to constrain circulation and mixing of past oceans [*Shackleton et al.*, 1988].

Figures 6 and 7 illustrate the dependence of the T and $\Delta^{14}C$ profiles from the low latitude ocean on each of the physical parameters. The three curves in each figure are solutions for $T_I(z)$ and $\Delta^{14}C_I(z)$ for 0.5, 1 and 1.5 times the best fit value of one parameter while the remaining three are held at their best fit values. Corresponding values for T_{HD}, $\Delta^{14}C_{LS}$, $\Delta^{14}C_{HS}$, and $\Delta^{14}C_{HD}$ are given in Table 4. Data-based T and $\Delta^{14}C$ profile constraints for the low latitude ocean

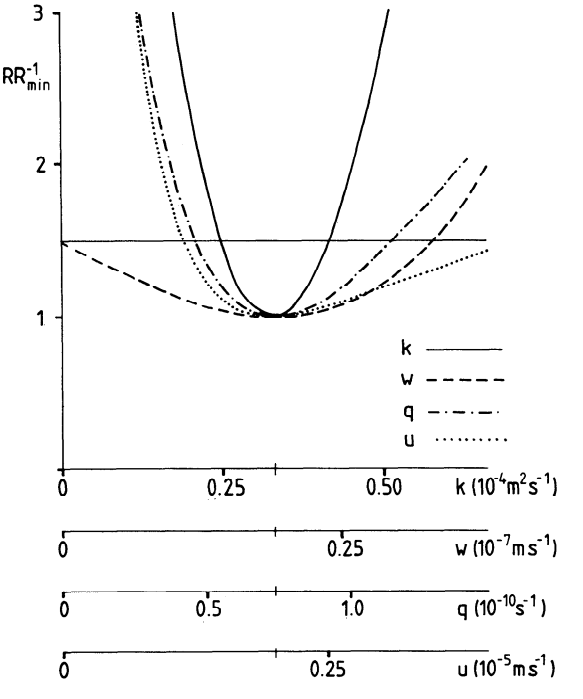

Figure 5. Ratios of minimum to absolute minimum residual (RR_{min}^{-1}) of HILDA model fits to temperature and carbon 14 data calculated by prescribing values for one of the free parameters while allowing the other three to vary. The x-axes have been scaled to make best fit values of these parameters coincide. The horizontal line marks RR_{min}^{-1} = 1.5.

Table 3. Best fit Solution Values for k, w, q and u for Several Different Combinations of Low- and High Latitude Surface Layer Temperature (T_{LS}, T_{HS}), Low- and High Latitude Surface Layer Carbon 14 ($\Delta^{14}C_{LS}$, $\Delta^{14}C_{HS}$), Atmospheric Carbon 14 ($\Delta^{14}C_A$) and Scaled, High Latitude, Air-Sea Exchange ($\delta_S g_{HS}(\delta g_{LS})^{-1}$).

T_{LS}, °C	T_{HS}, °C	T_{HD}, °C	$\Delta^{14}C_{LS}$ ‰	$\Delta^{14}C_{HS}$ ‰	$\Delta^{14}C_A$ ‰	$\delta_S g_{HS}$ $(\delta g_{LS})^{-1}$	g_{LS}, 10^{-5} m s^{-1}	k, 10^{-7} m^2 s^{-1}	w, 10^{-8} m s^{-1}	q, 10^{-11}s^{-1}	u, 10^{-6} m s^{-1}	RR_m^{-1}
19.54	-0.34	0.80	-40	-120	0	1	2.32	3.2	2.0	7.5	1.9	1.000
21.0*	-0.34	0.80	-40	-120	0	1	2.32	2.9	2.1	8.1	1.9	1.336
18.0*	-0.34	0.80	-40	-120	0	1	2.32	3.5	1.8	7.0	1.9	0.669
19.54	0.53*	0.80	-40	-120	0	1	2.32	3.2	2.3	6.7	3.0	1.179
19.54	-1.00*	0.80	-40	-120	0	1	2.32	3.3	1.7	8.1	1.5	0.922
19.54	-0.34	0.30*	-40	-120	0	1	2.32	3.3	2.0	7.2	2.0	1.144
19.54	-0.34	1.30*	-40	-120	0	1	2.32	3.2	1.9	7.7	1.8	0.914
19.54	-0.34	0.80	-30*	-120	0	1	2.76	2.7	1.1	7.3	2.0	0.826
19.54	-0.34	0.80	-40	-140*	0	1	2.19	3.1	0.4	10.2	2.8	0.795
19.54	-0.34	0.80	-40	-100*	0	1	2.47	3.3	3.0	5.9	1.3	1.460
19.54	-0.34	0.80	-50*	-120	0	1	2.00	3.7	2.8	7.6	1.8	1.186
19.54	-0.34	0.80	-40	-120	-5*	1	2.56*	3.1	1.8	7.5	1.9	0.971
19.54	-0.34	0.80	-40	-120	0	0.625*	2.69*	3.8	3.0	7.3	1.8	1.147
19.54	-0.34	0.80	-40	-120	0	1.600*	1.91*	2.7	0.9	7.6	2.0	0.864

Here g_{LS} and g_{HS} are low- and high-latitude air-sea exchange velocities, and δ and δ_S are total and ice-free area fractions at high latitudes. Also listed are g_{LS} and the ratio of the minimum residual to the standard case minimum (RR_{min}^{-1}). The top line gives the standard, best fit solution results. The * values were changed for each calculation.

from Table 2 are also shown in Figures 6 and 7 (heavy dots).

The results in Figures 6 and 7 and Table 4 help to interpret the sensitivity calculations presented above. Each parameter affects the vertical structure of $T_I(z)$ and $\Delta^{14}C_I(z)$ differently. The observed temperature gradient in the deep ocean is approximated better for $k > k_B$. Greater vertical eddy transport in the interior (k) leads to larger transports out of the low-latitude surface layer despite a weaker, near-surface gradient (Figures 6a and 7a). The deep ocean is heated and enriched with ^{14}C as a result. The ^{14}C difference across the low-latitude sea surface increases (Table 4), supporting increased air-sea exchange to match ^{14}C transport through the thermocline. For the standard case, 62.1% of total ^{14}C transport from atmosphere to ocean enters through the low-latitude sea surface, and 83.7% of total radioactive decay occurs in the low latitude interior. Thus about three fourths of the net ^{14}C supply to the interior enters through the low-latitude sea surface, while over half of the transport through the high-latitude sea surface is exported to the low-latitude interior. For the cases of $1.5k_B$ and $0.5k_B$ the low-latitude fraction of ^{14}C invasion is 65.5% and 56.4%, respectively. Note that $\Delta^{14}C_{HD}$ is quite sensitive to changes in k (Table 4) since concentrations in the deep polar box are strongly coupled to typical concentrations in the interior through lateral exchange.

An increase in deep circulation raises the thermocline, cools the deep ocean, and enhances the $\Delta^{14}C$ maximum at the ocean bottom (Figures 6b and 7b). The depth of the deep $\Delta^{14}C$ minimum is controlled mainly by k and w (Figures 7a to 7d). Larger k and smaller w lead to a deeper $\Delta^{14}C$ minimum, in better agreement with the data. A best fit calculation for ^{14}C only, given the $\Delta^{14}C$ constraints of Table 2 and with $u = u_B$ (u is insensitive to $\Delta^{14}C$ constraints; see below) yields an excellent fit (mean deviation of 1.7 ‰ from the data) for $k = 4.9\text{x}10^{-5}$ m^2 s^{-1}, $w = 1.5\text{x}10^{-8}$ m s^{-1} and $q = 4.8\text{x}10^{-11}$ s^{-1}.

An increase in lateral exchange (q) tends to homogenize the deep ocean while sharpening the near-surface gradients of the low-latitude ocean (Figures 6c and 7c). In fact, the rather strong dependence of interior $\Delta^{14}C$ levels on q can be traced mainly to increased near surface gradients and thereby increased diffusive flux from the surface to the interior. T_{HD} but not $\Delta^{14}C_{HD}$ is sensitive to changes in q (Table 4), a behavior opposite to that in the interior. The increase of $\Delta^{14}C$ in the interior together with a decrease of interior - deep polar box concentration difference with increasing q explains this behavior.

Finally, an increase in high-latitude exchange (u) leads to cooling of the deep polar box and the interior (Figure 6d). However, as $T_{HD} \rightarrow T_{HS}$ for large u, ocean thermal structure becomes less sensitive to changes in u. Both absolute values and vertical structure of $\Delta^{14}C$ in the interior are quite insensitive to changes in u (Figure 7d). As reflected in model results for surface layer $\Delta^{14}C$ (Table 4), changes in u slightly affect the net rate of ^{14}C transport from the atmosphere to

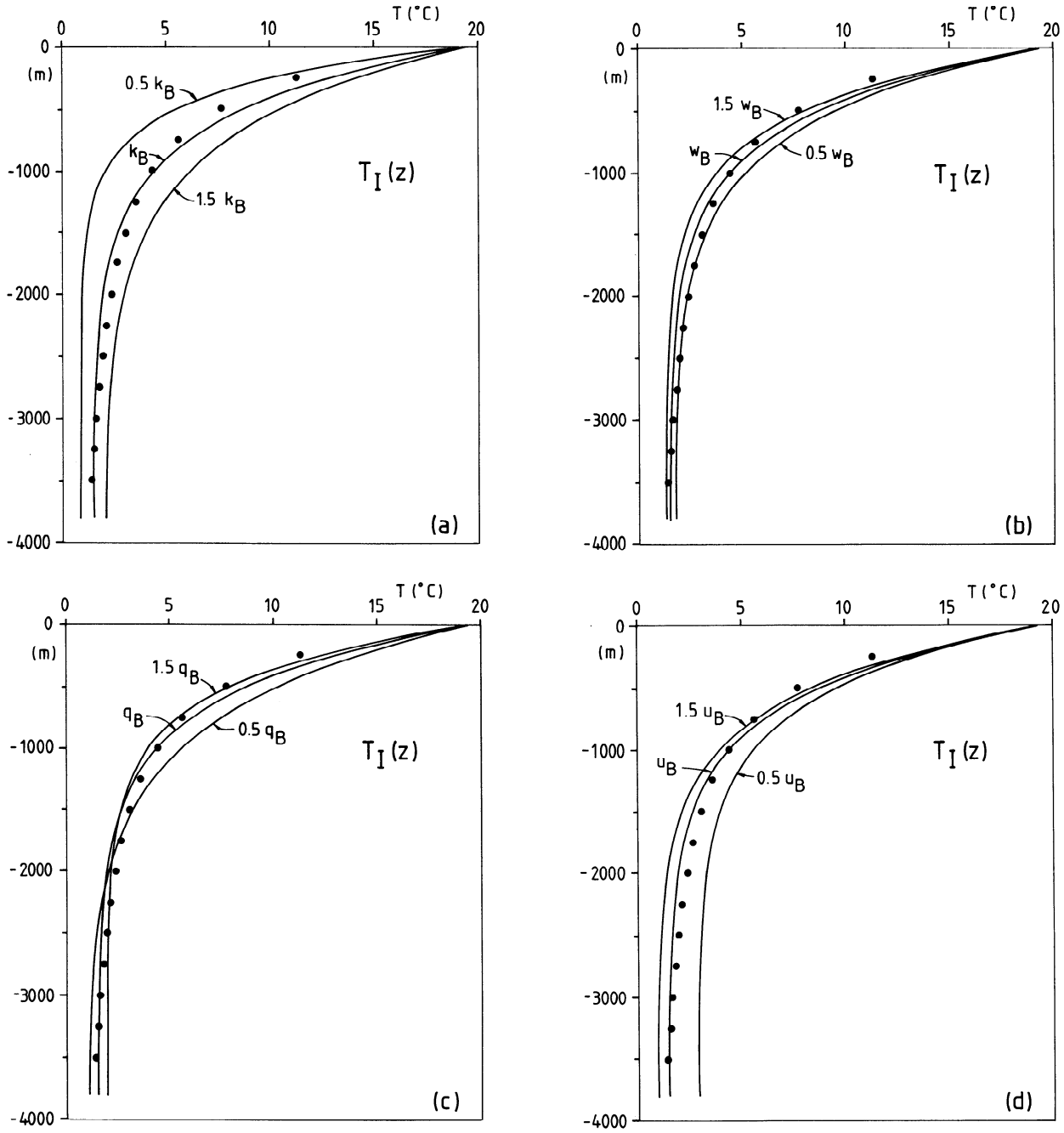

Figure 6. Model solutions for interior profiles of temperature for the low latitude ocean ($T_I(z)$) for 0.5, 1 and 1.5 times the best fit values of (a) k, (b) w, (c) q, and, (d) u where k_B, w_B, q_B and, $u_B = 3.2\text{x}10^{-5}$ m^2 s^{-1}, $2.0\text{x}10^{-8}$ m s^{-1}, $7.5\text{x}10^{-11}$ s^{-1} and $1.9\text{x}10^{-6}$ m s^{-1}. Also shown are data-based, mean potential temperatures from Figure 2 and Table 2 (dots).

the ocean. These results imply that at high latitudes, this transport is limited mainly by air-sea exchange given the vigorous exchange between surface and deep polar boxes. This contrasts sharply with the sensitivity of $\Delta^{14}C_{LS}$ and ^{14}C transport into the interior to changes in internal mixing and near surface $\Delta^{14}C$ gradients. Thus model results indicate that weak exchange through the thermocline, not air-sea exchange, is the main step limiting ^{14}C invasion into the low-latitude ocean.

Discussion

What are the physical analogs in the real ocean to the HILDA physical parameters, and what can we learn from best fit values of these parameters? Besides small-scale turbulence, k will include mid-latitude ventilation processes, since k will be sensitive to eddies on all horizontal scales up to the size of the HILDA interior box. *Siegenthaler and Joos* [1992] discuss this in more detail. The parameter w can be

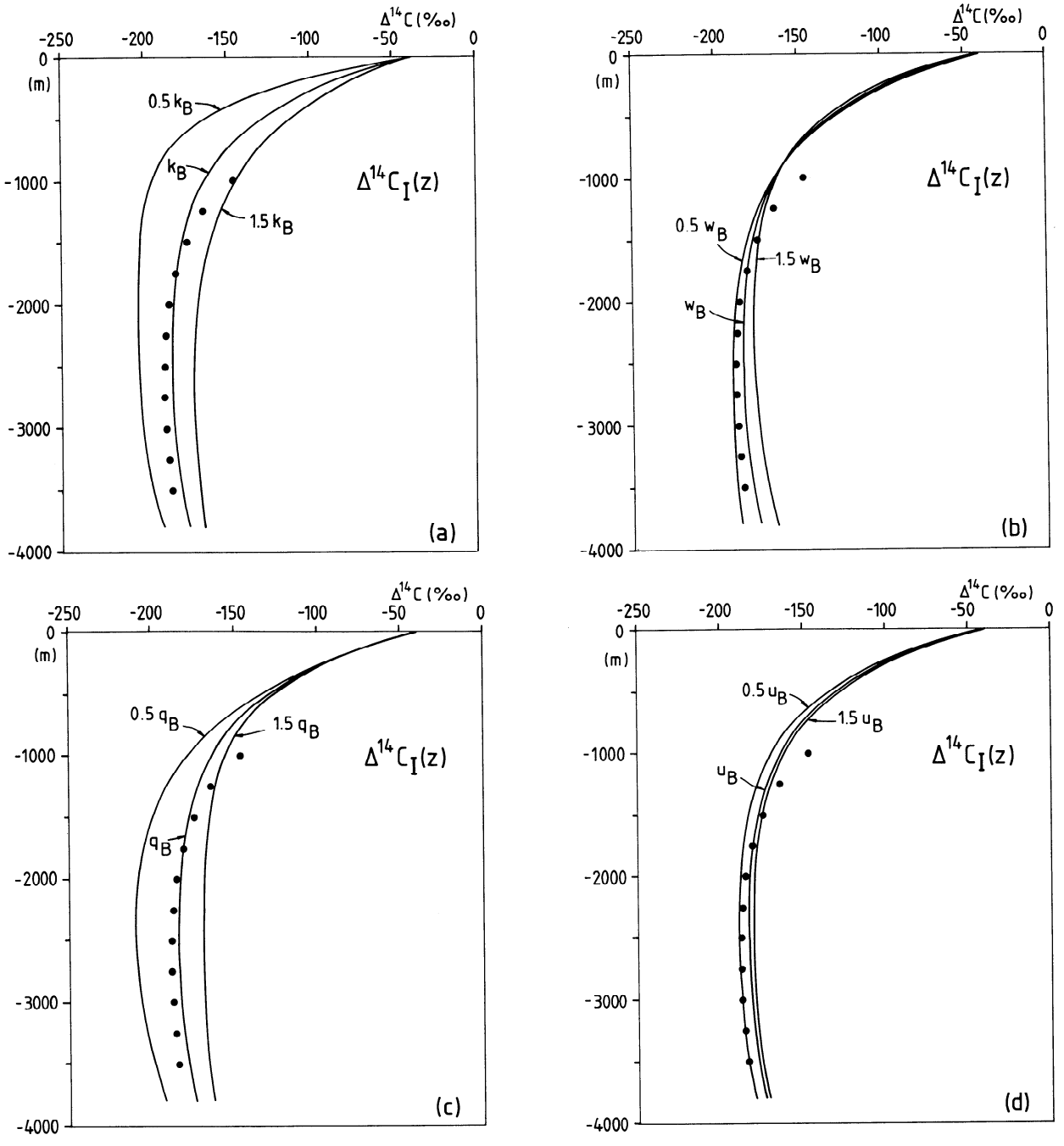

Figure 7. Model solution for interior profiles of carbon 14 for the low-latitude ocean ($\Delta^{14}C_I(z)$) for 0.5, 1, and 1.5 times the best fit values of (a) k, (b) w, (c) q, (d) u. Also shown data-based, mean carbon 14 curves from Figure 4 and Table 2 (heavy curve).

identified with the part of the deep, dense water formed in high-latitude surface layers which returns to the sea surface at low and middle latitudes. The parameter q might be identified with processes like entrainment into this dense water to complete the deep water formation and deep recirculation between high latitudes and the interior. Both q and u would be involved in the deep recirculation cell formed by upwelling into the Southern Ocean surface layer and the return flow to the deep ocean. The rest of u may be thought of as turbulent or convective exchange with shorter time and space scales. Below, we compare with results from simpler and more complex ocean models to help put our results in a proper perspective.

In the one-dimensional, box-diffusion model all physical transport processes in the ocean are lumped into k whereby a value of 13×10^{-5} $m^2 s^{-1}$ is needed to simulate observed deep $\Delta^{14}C$ levels [*Oeschger et al*, 1975]. The HILDA model contains an important interaction, missed in one-dimensional models but important in the real ocean: Strong, lateral ventilation (q in HILDA) combined with strong surface

Table 4. Model Solutions for the Temperature in the Deep Polar Ocean (T_{HD}) and for Carbon 14 in the Low- and High Latitude Surface Layers and the Deep Polar Ocean ($\Delta^{14}C_{LS}$, $\Delta^{14}C_{HS}$ and $\Delta^{14}C_{HD}$) for 0.5, 1 and 1.5 times the best fit values of k,w, q and u.

	T_{HD} °C	$\Delta^{14}C_{LS}$, 0/00	$\Delta^{14}C_{HS}$, 0/00	$\Delta^{14}C_{HD}$, 0/00
$0.5k_B$	0.94	-34.4	-140.6	-163.6
k_B	1.56	-39.0	-125.1	-145.0
$1.5k_B$	2.01	-41.8	-115.6	-133.7
$0.5w_B$	1.78	-37.3	-132.5	-151.3
w_B	1.56	-39.0	-125.1	-145.0
$1.5w_B$	1.36	-40.7	-118.1	-138.9
$0.5q_B$	0.94	-37.9	-124.7	-144.6
q_B	1.56	-39.0	-125.1	-145.0
$1.5q_B$	2.01	-40.2	-122.2	-141.6
$0.5u_B$	2.98	-40.4	-115.5	-151.9
u_B	-1.56	-39.0	-125.1	-145.0
$1.5u_B$	0.99	-38.5	-128.7	-142.4

Best fit values are k_B=3.2 x 10^{-5} m^2 s^{-1}, w_B = 2.0 x 10^{-8} m s^{-1}, q_B = 7.5 x 10^{-11} s^{-1}, and u_B = 1.9 x 10^{-6} m s^{-1}.

sources or sinks sharpens near-surface gradients whereby even moderate levels of eddy activity can lead to significant diffusive transport across the ocean thermocline. As a result of this effect, our best fit solution exhibits a "diffusive" transport of ^{14}C into the interior ($kd^{14}C_I(z)/dz \mid_{z=0}$) about 3/4 as large as that required in the purely "diffusive" box diffusion model but supported by k levels (3.2x10^{-5} m^2 s^{-1}) only about 1/4 as large as required in that model.

A one-dimensional, advection-diffusion approach to fit ocean mean $\Delta^{14}C$, T and salinity profiles leads to "canonical" values of the order of 10x10^{-5} m^2 s^{-1} for k and 10x10^{-8} m s^{-1} for the deep advection w [*Munk*, 1966; *Broecker and Peng*, 1982]. With the upwelling transport given by $(1-\delta)wA$, where A, the ocean surface area, is 3.60x10^{14} m^2, this value for w implies a transport of 30 Sv, 5 times as large as our HILDA estimate of 6.0 Sv given w_B = 2.0x10^{-8} m s^{-1}. In fact, we found a reasonably good fit to tracer data considered here for $w \rightarrow 0$. On the other hand, the transport associated with q_B is $(1-\delta)q_BDA$ = 86.2 Sv. Model fit to data was found to degrade rapidly for transports less than about 50 Sv associated with q. Thus our analysis indicates that deep recirculation (the analog to q) rather than deep upwelling (the analog to w) dominates the deep ventilation of the global ocean.

One way to evaluate these conclusions is to compare with results of a recent steady state, ocean general circulation model simulation (OGCM) of natural ^{14}C [*Toggweiler et al.*, 1989, hereinafter referred to as TDB]. As calculated by *Siegenthaler and Joos* [1992], the mean vertical advection from the TDB results for the region corresponding to the HILDA interior actually turns out to be negative at almost all depths. The transport streamline of the zonally integrated overturning in the TDB simulation (their Figure 4) showed the exchange between polar and low-mid latitude regions in the OGCM to be dominated by deep recirculation cells carrying a total of about 50 Sv and including two deep, counterrotating cells fed by upwelling of about 30 Sv into the surface layer of the Southern Ocean. Thus the OGCM results also indicate that deep recirculation reigns over upwelling in the deep ocean.

A comparison of the ocean mean $\Delta^{14}C$ profile from the TDB prognostic model with data (their Figure 8) shows too much ^{14}C in the ocean thermocline (by about 20-30 ‰) but too little ^{14}C in the deep ocean (by about 20-30 ‰). The first problem, also found for temperature (up to 4°C warmer than observations in the ocean thermocline), probably reflects excessive ventilation of mid-latitude surface water and/or too large a choice for vertical eddy diffusivity. *Siegenthaler and Joos* [1992] used TDB model output to estimate effective vertical diffusivity for the HILDA geometry due to mid-latitude ventilation and found a value of about 6x10^{-5} m^2 s^{-1} for natural ^{14}C in the ocean thermocline. In the TDB model, k, a parameterization of the effects of sub-grid scale eddies (in this case several hundred kilometers or less), is taken to lie between 3x10^{-5} m^2 s^{-1} and 11x10^{-5} m^2 s^{-1} from ocean surface to bottom. Estimates of k from microstructure measurements in the ocean thermocline are typically 1x10^{-5} m^2 s^{-1} or less [*Moum and Osborne*, 1986]. A reduction of midlatitude ventilation and/or k in the TDB model would improve agreement with thermocline $\Delta^{14}C$ data and with our HILDA value of 3.2x10^{-5} m^2 s^{-1} for k. However, Siegenthaler and Joos argue that this value may be somewhat low because of our simulaneous fit to T and $\Delta^{14}C$ data. Indeed, our best fit k value to the $\Delta^{14}C$ data alone was about 5x10^{-5} m^2 s^{-1}.

The problem of too little ^{14}C in the deep layers of the TDB model reflects insufficient deep ventilation. For instance, the flow of North Atlantic Deep Water is too shallow in the TDB model. More vigorous deep recirculation and/or deep upwelling would be needed to fit the deep $\Delta^{14}C$ data. Best fit HILDA results for q_B indicate that more vigorous deep recirculation would be in better agreement with the real ocean. *Bryan* [1987] showed that vertical overturning in coarse-resolution OGCMs like that used by TDB is sensitive to the choice of k. A larger value for k in the TDB model would lead to greater vertical overturning and deep ventilation but also greater mismatch between model results and temperature and $\Delta^{14}C$ data in the ocean thermocline.

The transport associated with the vertical exchange between the surface and deep layers at high latitudes in the HILDA model is δu_BA. For u_B=1.9x10^{-6} m s^{-1}, this transport is 109.4 Sv. Our model fit to data degraded rapidly for transports less than about 60 Sv associated with u. For a three-box model of ocean chemistry with high-latitude

dynamics, calibrated by ocean data (^{14}C, phosphate and, oxygen) and by atmospheric pCO_2, *Toggweiler and Sarmiento* [1985] found lower values for this transport: 45 - 60 Sv. On the other hand, their deep circulation was 19 Sv compared to our value of 6 Sv. Here with HILDA, we have been able to make use of additional information contained in the deep interior profile of $\Delta^{14}C$ (Figure 7b) to constrain the deep circulation. Given weak deep circulation and weak turbulent mixing required to fit strong T and ^{14}C gradients in the ocean thermocline, strong exchange is needed between the high latitude surface layer and the interior of the low latitude ocean to cool the interior and to supply it with enough ^{14}C.

Here we neglected bidirectional exchange between the high- and low-latitude surface layers, an exchange taken to be 10 Sv in *Toggweiler and Sarmiento* [1985]. A lower bound for this exchange might be $(1-\delta)q_B HA$ where H is a surface layer depth. With H equal to 75 m, this is 1.5 Sv. If this value is doubled to simulate greater eddy activity in the upper ocean like choices often made in OGCM's like in TDB, such exchange would only modify net fluxes in and out of the model surface layers by at most 10% for our solutions. For this reason and since we obtained good fits to data with our basic model, we neglected this term and thereby avoided another free parameter in our model.

It is unsatisfying that the upper bound of u is rather poorly constrained by the T and $\Delta^{14}C$ data (Figure 5) and is quite sensitive to the choice of T_{HS}. In a time-dependent, numerical calculation based on the HILDA model, *Joos et al.* [1991] found u to be constrained more tightly by CFC-11 inventories in the Southern Ocean. Although their model differs from ours in several aspects, their result for u of 1.2 $\pm 0.5 \times 10^{-6}$ m s^{-1} or about 70 ± 30 Sv indicates that we have not underestimated the appropriate value for u and that a "cold," wintertime choice for T_{HS} is reasonable.

Clearly, the HILDA model greatly oversimplifies ocean physics. Still, the above analysis indicates that this new model may capture the essence of flow and exchange between and within low- and high-latitude portions of the global ocean with only four free parameters. As shown here, ocean-averaged data of temperature and carbon 14 put significant constraints on the values of these four parameters for the modern ocean, values which compare rather well with analogs derived from much more complex models. From these results we conclude that the HILDA model forms a useful framework with well-constrained physics for studying biogeochemical cycling in the global ocean. This is demonstrated in papers 2 and 3 of this series.

Appendix

This appendix gives algebraic equations from the application of HILDA model conservation equations for boundary boxes and boundary and matching conditions given the HILDA general solution for temperature T and ^{14}C in the interior of the low-latitude ocean. $A_{1,2}$ and $B_{1,2}$ are constants of the general solutions. See text and figure 1 for definition of other symbols.

Temperature

$$T_{LS}-T_{HD}-A_1-B_1 = 0 \quad \text{(A1)}$$

$$A_1(ks_1-w)\exp(-s_1 D)+B_1(ks_2-w)\exp(-s_2 D) = 0 \quad \text{(A2)}$$

$$w(T_{HS}-T_{LS})+\delta(1-\delta)^{-1}u(T_{HS}-T_{HD}) \quad \text{(A3)}$$
$$+ks_1A_1+ks_2B_1 = 0$$

where s_1, $s_2=0.5[wk^{-1}\pm(w^2k^{-2}+4qk^{-1})^{1/2}]$.

Carbon 14

$$^{14}C_{LS}-q(q+\lambda)^{-1}(^{14}C_{HD})-A_2-B_2 = 0 \quad \text{(A4)}$$

$$A_2(ks_3-w)\exp(-s_3 D)+B_2(ks_4-w)\exp(-s_4 D) \quad \text{(A5)}$$
$$+\lambda w(q+\lambda)^{-1}(^{14}C_{HD}) = 0$$

$$g_{LS}(1-^{14}C_{LS})-ks_3 A_2-ks_4B_2 = 0 \quad \text{(A6)}$$

$$\delta_S g_{HS}(1-^{14}C_{HS})+(1-\delta)w(^{14}C_{LS}-^{14}C_{HS}) \quad \text{(A7)}$$
$$-\delta u(^{14}C_{HS}-^{14}C_{HD}) = 0$$

$$q[(1-\delta)g_{LS}+\delta_S g_{HS}]-q(1-\delta)g_{LS}{}^{14}C_{LS} \quad \text{(A8)}$$
$$+^{14}C_{HS}[(1-\delta)\lambda w+\delta\lambda u-q\delta_S g_{HS}]$$
$$-\lambda{}^{14}C_{HD}[(1-\delta)w+\delta u+D(q+\delta\lambda)] = 0$$

where s_3, $s_4=0.5\ [wk^{-1}\pm(w^2k^{-2}+4(q+\lambda)k^{-1})^{1/2}]$.

Acknowledgements. We wish to thank Teresa Fierro Pedreros, Agneta Malm, and Ola Åkerlund for help in the preparation of this manuscript. Discussions with Robbie Toggweiler and Ray Najjar were valuable. Part of this work was carried out while the first author was a Visiting Senior Research Scientist at the Program for Atmospheric and Oceanic Sciences, Princeton University. This study was supported by the Program, NSF grant OCE 8711905, and grants from the geoscience division of the Swedish Natural Science Research Council.

References

Bacastow, R., and E. Maier-Reimer, Ocean-circulation model of the carbon cycle, *Clim. Dyn.*, *4*, 95-125, 1990.

Barnola, J.M., D.Raynand, Y.S. Korotkevich, and C. Lorius Vostok ice cores provides 160,000 year record of atmospheric CO_2, *Nature*, *329*, 408-414, 1987.

Bolin, B., How much CO_2 will remain in the atmosphere? in: *The Greenhouse Effect, Climatic Change and Ecosystems*, SCOPE vol. 29, edited by B. Bolin, B.R. Döös, J. Jäger, and R.A. Warrick, 93-156, John Wiley, New York, 1986.

Broecker, W.S., Ocean chemistry during glacial times, *Geochim.et Cosmochim Acta*, *46*, 1689-1705, 1982.

Broecker, W.S. and T.-H. Peng, *Tracers in the Sea*, 690 pp.,

Lamont-Doherty Earth Observatory, Columbia University, New York, 1982.

Bryan, F., Parameter sensitivity of primitive equation ocean general circulation models, *J. Phys. Oceanogr.*, *17*, 970-985, 1987.

Fanning, K.A and L.M. Torres, ^{222}Rn and ^{226}Ra: in dicators of sea-ice effects on air-sea gas exchange, *Polar Res.*, *10*, 51-58.

Fiadeiro, M.E., Three-dimensional modeling of tracers in the deep Pacific Ocean, II, Radiocarbon and the circulation, *J. Mar. Res.*, *40*, 537-550, 1982.

Gordon, A.L., Seasonality of Southern Ocean sea ice, *J. Geophy. Res.*, *86*(C5), 4193-4197, 1981.

Joos, F., U. Siegenthaler, and J.L. Sarmiento, Possible effects of iron fertilization in the Southern Ocean on atmospheric CO_2 concentration, *Global Biogeochem. Cycles*, *5*, 135-150, 1991.

Knox, F., and M.B. McElroy, Changes in atmospheric CO_2: Influence of the marine biota at high latitude, *J. Geophys. Res.*, *89*, 4629-4637, 1984.

Levitus, S., Climatological atlas of the world ocean, *NOAA Prof. Pap.*, *13*, US Gov. Print. Off., Washington D.C., 1982.

Manabe, S. and K. Bryan, CO_2-induced change in a coupled ocean-atmosphere model and its paleoclimatic implications, *J. Geophys. Res.*, *90*, (C6), 11,689-11,707, 1985.

Moum, J.N. and T.R. Osborne, Mixing in the main thermocline, *J. Phys. Oceanog.*, *16*, 1250-1259, 1986.

Munk, W.H., Abyssal recipes., *Deep- Sea Res.*, *13*, 707-730, 1966.

Neftel, A., H. Oeschger, J. Schwander, G. Stauffer, and R. Zumbrunn, Ice core measurements give atmospheric CO_2 content during the past 40,000 yr., *Nature*, *295*, 220-223, 1982.

Oeschger, H., U. Siegenthaler, U. Schotterner, and A. Grugelmann, A box-diffusion model to study the carbon dioxide exchange in nature, *Tellus*, *27*, 168-192, 1975.

Peng, T.-H., W.S. Broecker, G.G. Matheu, Y.-H. Li, and A.E. Bainbridge, Radon evasion rates in the Atlantic and Pacific Oceans as determined during the GEOSECS program, *J. Geophys. Res.*, *84* (C5), 2471-2486, 1979.

Sarmiento, J.L., and J.R. Toggweiler, A new model for the role of the oceans in determining atmospheric pCO_2, *Nature*, *308*, 621-624, 1984.

Shackleton, N.J., J.-C. Duplessy, M. Arnold, P. Maurice, M.A. Hall, and J. Cartlidge, Radiocarbon age of the last glacial Pacific deep water, *Nature*, *335*, 708-711, 1988.

Shaffer, G., A model of biogeochemical cycling of phosphorus, nitrogen, oxygen, and sulphur in the ocean: One step toward a global climate model, *J. Geophys. Res.*, *94*(C2), 1979-2004, 1989.

Siegenthaler, U., Uptake of excess CO_2 by an outcrop-diffusion model of the ocean, *J. Geophys. Res.*, *88*(C6), 3599-3608, 1983.

Siegenthaler, U., Carbon dioxide: its natural cycle and anthropogenic perturbation, in: *The Role of Air-Sea Exchange in Geochemical Cycling*, edited by P. Buat-Menard, pp. 209-247, D. Reidel, Norwell, Mass., 1986.

Siegenthaler, U., and F. Joos, Use of a simple model for studying oceanic tracer distributions and the global carbon cycle, *Tellus, Ser. B*, *44*, 186-207, 1992.

Siegenthaler, U. and T. Wenk, Rapid atmospheric CO_2 variations and ocean circulation, *Nature*, *308*, 624-626, 1984.

Stuiver, M. and P.D. Quay, Changes in atmospheric carbon-14 attributed to a variable Sun, *Science*, *207*, 11-19, 1980.

Stuiver, M., P.D. Quay, and H.G. Ostlund, Abyssal water carbon-14 distribution and the age of the world oceans, *Science*, 219, 849-851, 1983.

Toggweiler, J.R., and J.L. Sarmiento, Glacial to interglacial changes in atmospheric carbon dioxide: Critical role of ocean surface water in high latitudes, in: *The Carbon Cycle and Atmospheric CO_2: Natural Variations Archean to Present*, edited by E.T. Sundquist and W.S. Broecker, *Geophys. Monogr. Ser.*, vol. 32, pp. 163-184, AGU, Washington, D.C., 163-184, 1985.

Toggweiler, J.R., K. Dixon, and K. Bryan, Simulations of radiocarbon in a coarse-resolution world ocean model 1, Steady state prebomb distributions, *J. Geophys.Res.*, *94*, (C6), 8217-8242, 1989.

Volk, T., and M.I. Hoffert, Ocean carbon pumps: analysis of relative strengths and efficiencies in ocean-driven atmospheric pCO_2 change, in: *The Carbon Cycle and Atmosphere CO_2: Natural Variations Archean to Present, Geophys. Monogr. Ser.*, vol 32, edited by E.T. Sundquist and W.S. Broecker, pp. 99-110, AGU, Washington, D.C., 1985.

Walsh, J.E., and C.M. Johnson, An analysis of Arctic sea ice fluctuations, *J. Phys. Oceanogr.*, *9*, 580-591, 1979.

Jorge L. Sarmiento, Program in Atmospheric and Oceanic Sciences, Princeton University, P.O. Box 308, Princeton, NJ 08542, USA.

Gary Shaffer, Department of Geophysics, Niels Bohr Institute for Astronomy, Physics and Geophysics, University of Copenhagen, Haraldsgade 6, DK-2200 Copenhagen N, Denmark.

(Received May 13, 1993; revised March 20 1994;
accepted April 25, 1994.)